aerospace

MDPI

Article

Aerodynamic Data-Driven Surrogate-Assisted Teaching-Learning-Based Optimization (TLBO) Framework for Constrained Transonic Airfoil and Wing Shape Designs

Xiaojing Wu [1,2,*], Zijun Zuo [1] and Long Ma [1]

[1] School of Civil Aviation, Northwestern Polytechnical University, Xi'an 710072, China
[2] Yangtze River Delta Research Institute, NPU, Taicang 215400, China
* Correspondence: wuxj@nwpu.edu.cn

Abstract: The surrogate-assisted optimization (SAO) process can utilize the knowledge contained in the surrogate model to accelerate the aerodynamic optimization process. The use of this knowledge can be regarded as the primary form of intelligent optimization design. However, there are still some difficulties in improving intelligent design levels, such as the insufficient utilization of optimization process data and optimization parameters' adjustment that depends on the designer's intervention and experience. To solve the above problems, a novel aerodynamic data-driven surrogate-assisted teaching-learning-based optimization (TLBO) framework is proposed for constrained aerodynamic shape optimization (ASO). The main contribution of the study is that ASO is promoted using historically aerodynamic process data generated during the gradient free optimization process. Meanwhile, nonparametric adjustment of the TLBO algorithm can help relieve manual design experience for actual engineering applications. Based on the structure of the TLBO algorithm, a model optimal prediction method is proposed as the new surrogate-assisted support strategy to accelerate the ASO process. The proposed method is applied to airfoil and wing shape designs to verify the optimization effect and efficiency. A benchmark aerodynamic design optimization is employed for the drag minimization of the RAE2822 airfoil. The optimized results indicate that the proposed method has advantages of high efficiency, strong optimization ability, and nonparametric characteristics for ASO. Moreover, the results of the wing shape optimization verify the advantages of the proposed methods over the surrogate-based optimization and direct optimization frameworks.

Keywords: aerodynamic shape optimization; aerodynamic data; surrogate-assisted optimization; TLBO algorithm; AIAA aerodynamic optimization benchmark

Citation: Wu, X.; Zuo, Z.; Ma, L. Aerodynamic Data-Driven Surrogate-Assisted Teaching-Learning-Based Optimization (TLBO) Framework for Constrained Transonic Airfoil and Wing Shape Designs. *Aerospace* **2022**, *9*, 610. https://doi.org/10.3390/aerospace9100610

Academic Editor: Simão Marques

Received: 16 August 2022
Accepted: 12 October 2022
Published: 17 October 2022

1. Introduction

Aerodynamic design has become an essential research topic in aeronautical engineering, particularly in modern civil aircraft designs. With the rapid development of computational technologies, aerodynamic shape optimization (ASO), which combines computational fluid dynamics (CFD) with numerical optimization, has been widely employed for aerodynamic designs in the last 40 years [1,2]. Advantageously, ASO can effectively overcome the shortcomings of the traditional "Try and On" methods and greatly improve the automatic level of aerodynamic designs.

To date, various optimization methods have been developed pertaining to ASO. They can be mainly divided into two categories: gradient-based and gradient-free methods. Adjoint-based algorithms are widely utilized in gradient-based methods, as they only need to solve the flow field once to obtain the gradient information of the objective and constraint function for all design variables [3–10]. Based on the gradient information, adjoint-based algorithms exhibit high optimization efficiencies. However, they have the disadvantage of falling into local optimum, which often depends on the selection of the optimization starting points. To overcome this shortcoming, gradient-free methods, such as global

evolutionary algorithms, are also widely used for ASO. However, the direct optimization (DO) framework that the evolutionary algorithm utilizes to directly employ CFD tools for ASO is unsuitable for engineering aerodynamic design due to the expensive computational cost of the CFD evaluation and the very low efficiency of the evolutionary algorithm. For example, the computational cost of a CFD simulation for an airplane shape is approximately tens of hours. Thus, the computational cost is unacceptable and hinders the use of the DO framework for achieving global optimization for actual aeronautical engineering designs.

Surrogate model techniques have been introduced in ASO to improve the efficiency of gradient-free methods. Surrogate-based optimization (SBO) [11] is the most popular ASO framework, which aims to establish an approximate surrogate model that is equivalent to the expensive CFD simulations in the design space through the design of experiments; then, a global optimization algorithm optimizes the approximate surrogate model for ASO. Various SBO methods have been developed because the optimization efficiency of the SBO framework can be considerably improved, e.g., iterative response surface-based optimization [12], multiple-surrogate approach [13], multistage metamodeling approach [14], adaptive SBO [15,16] and variable-fidelity surrogate modeling [17,18]. In addition to SBO frameworks, another ASO framework that employs surrogated model techniques is surrogate-assisted optimization (SAO), wherein global optimization algorithms are modified using surrogate models to accelerate the optimization process. Currently, the research on SAO is relatively elementary in the field of ASO. The inexact pre-evaluation (IPE) strategy is developed to assist the global optimization algorithms (GA and PSO), with the aim of accelerating the aerodynamic optimization process [19–24]. That is, the offspring population individuals are sorted and selected based on the IPE of the surrogate model. Then, these selected individuals are evaluated according to real CFD evaluations and used for genetic operations to produce the next generation population.

In these two surrogate models, the SBO framework does not change the structure of its optimization algorithms. It finds the optimal solution by improving the accuracy of the constructed surrogate model. Thus, disadvantageously, its optimization results highly depend on the accuracy of the constructed surrogate model and the sample infilling strategies. SAO must change the structure of the global optimization algorithms. The knowledge contained in the surrogate models can be used to guide the optimization search by constantly learning perfect knowledge and experience from the model in the SAO frameworks. Compared to SBO, SAO can advantageously reduce the dependence on the surrogate model, as new individuals selected by the surrogated model are directly evaluated by CFD in the selection operation to produce the next generation's population. SAO frameworks still have great development potential for ASO design, owing to their advantages.

The optimization process of the global evolutionary algorithm generates considerable aerodynamic data. These aerodynamic data are generated during real CFD simulations with the evolutionary optimization process. Particularly, the individuals that fail in the competition are never reused in the after-optimization process, but they may contain useful information for promoting the aerodynamic optimization process. To the best of our knowledge, the current aerodynamic optimization methods do not fully utilize these historical process data to support the aerodynamic optimization design. Thus, this study aims to develop an effective method for reusing these historical process aerodynamic data and extract useful information from them to guide the aerodynamic design optimization process.

In addition, parameter-free adjustment can be considered as another work worthy of consideration to realize intelligent optimization design. The above ASO mainly focuses on the improvement of DE, PSO, and GA algorithms. In these common heuristic algorithms, there are some corresponding parameters of these heuristic algorithms that must be set according to different optimization problems. For example, PSO should adjust inertia weight, social, and cognitive parameters; GA and DE should adjust crossover and mutation rate parameters. The optimal tuning of these parameters is crucial for successful optimization. Otherwise, it might unnecessarily increase the computational effort or become stuck at local optimal solutions if these parameters are irrational. The adjustment of these

parameters often depends on the experience of designers or experts, which results in inconvenience of use in the actual complex engineering optimization designs. Moreover, it still must set corresponding parameters according to different optimization problems, which is obviously inconvenient to engineering uses. Recently, Rao [25] proposed a teaching-and-learning-based optimization (TLBO) algorithm; it is a nonparametric algorithm and can handle nonlinear problems well. Moreover, no parameter, other than the population size (N_p), needs to be adjusted during its optimization process. The TLBO algorithm has been developed and used to solve complex optimization problems due to its excellent characteristics [26–29]. Qu [30] first proposed a novel TLBO memetic algorithm (TLBO-MA) based on the SBO framework for ASO to improve the searching performance and comprehensive optimization capability of TLBO. In our previous study, we proposed a data-driven TLBO framework for unconstrained expensive engineering optimization problems [31].

Motivated by the above discussion, a new aerodynamic data-driven surrogate-assisted optimization framework with the TLBO algorithm is proposed for aerodynamic designs from the data-driven perspective by fully utilizing the historical aerodynamic data generated during the optimization process. Aerodynamic shape designs are often constrained optimization problems due to the complex engineering design requirements. For example, the constraints of lift and moment must be considered when optimizing the drag reduction of the wing in ASO. Aerodynamic data are generated by the CFD simulation using the TLBO algorithm. The online surrogate model is adaptively learned using these aerodynamic data, which are used to guide and accelerate the aerodynamic optimization process. Finally, to verify the optimization effect and efficiency, the proposed DDSAO framework is applied to constrained aerodynamic optimization designs for transonic drag minimization of RAE2822 airfoil and three-dimensional (3-D) wings. The optimization effect and efficiency of ASO can be improved from the perspectives of data-driven methods.

The rest of the paper is organized as follows: Section 2 introduces the ASO. The developed DDSAO framework is comprehensively introduced in Section 3. In Section 4, a benchmark ASO is conducted for the drag minimization of the RAE2822 airfoil in the transonic viscous flow using the DDSAO method. Additionally, comparisons are performed with other optimization methods and other benchmark results. In Section 5, ASO is performed for a 3-D wing shape design. Lastly, the conclusions are presented in Section 6.

2. Materials and Methods

Since the 1970s, when Hick and Henne pioneered the aerodynamic shape design, the combination of CFD and optimization techniques has become a powerful and reliable technical tool for solving aerodynamic shape design problems. Subsequently, aerodynamic designs have evolved from "Try-and-On" methods relying on wind tunnel tests and designers' experiences to the ASO methods integrating CFD and numerical optimization methods. ASO combines modern CFD technology with numerical optimization algorithms to automatically obtain an optimal aerodynamic shape using a computer. It is multidisciplinary research involving aerodynamics, computer technologies, optimization methods, modeling technologies, etc. Figure 1 displays the flow of the aerodynamic design optimization and its contents. The research involved in ASO mainly includes the following three aspects: establishment of the optimization model, the optimization methods, and the evaluation of the aerodynamic characteristics. In this section, the optimization model is established, and the aerodynamic characteristics are evaluated for ASO.

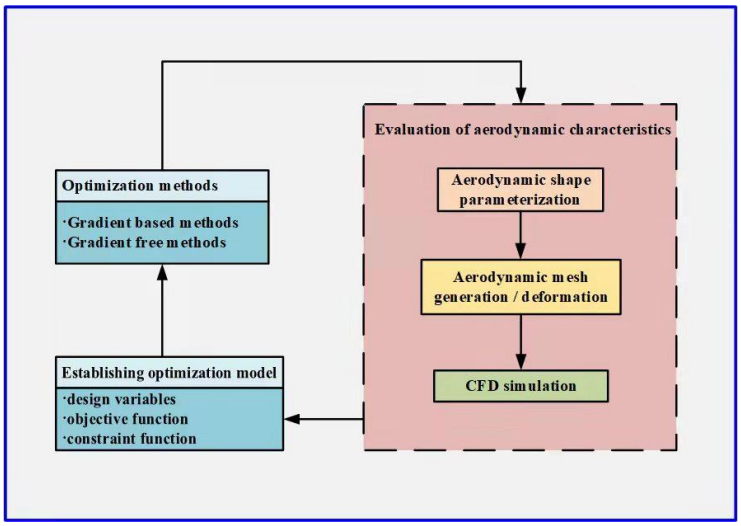

Figure 1. ASO framework.

2.1. Establishment of the Optimization Model

In the ASO framework, a mathematical model of the optimization design must first be established according to the specific engineering design requirements. The optimization model is established according to the specific aerodynamic design requirements of the aircrafts in the ASO framework. It is usually a constrained optimization problem due to the complex characteristics of aircraft design. Thus, the establishment of the optimization model includes the determination of the design variables, constraints, and objective functions. The constrained optimization model can be described using Equation (1):

$$\begin{gathered} Min\ f(\mathbf{x}) \\ s.t.\ g_i(\boldsymbol{x}) \le 0\ \ (i = 1, 2, \ldots, I) \\ \boldsymbol{x_L} \le \boldsymbol{x} \le \boldsymbol{x_U} \end{gathered} \tag{1}$$

where $f(\mathbf{x})$ denotes the objective function, which is usually expressed as drag coefficient C_d; $g_i(\boldsymbol{x})$ denotes the constraint function, which is usually expressed as the Lift coefficient C_l and moment coefficient C_m; and $\boldsymbol{x}$ denotes the design variables, which is usually expressed as the shape parameter. In ASO design, a problem that is usually encountered is that the objective and constraint functions usually need to be considered in the evaluation of aerodynamic characteristics. For example, the constraints of lift and moment coefficients usually need to be considered in ASO for drag reduction. Thus, to improve the optimization efficiency, the surrogate models of the drag, lift, and moment coefficients must be established.

To solve the constrained optimization problem, the penalty function method is used to transform the constrained problem into an unconstrained problem herein. The converted objective corresponding to these aerodynamic models is expressed as follows:

$$F(x) = f(x) + \frac{1}{\mu}\left(\sum_1^I Max(g_i(x), 0)\right) \tag{2}$$

where μ ($\mu \ll 1$) is the penalty factor.

2.2. Optimization Methods

The optimization method is an important part of aerodynamic shape design optimization, and it directly determines the optimization effect on the aerodynamic shape design. In particular, the aero-optimization method is an important part of the aerodynamic shape optimization design. The development of efficient optimization methods with

high search capability is one of the most important research tasks in aerodynamic shape design optimization.

The gradient optimization algorithm has become the most widely used optimization method owing to its high optimization efficiency. In gradient optimization algorithms, the solving of the gradient information of the objective and constraint functions has a certain impact on the efficiency of the optimization. Since the adjoint algorithm only needs to solve the flow field once to obtain the gradient information of the objective or constraint functions for all design variables, the computational effort of the adjoint algorithm to solve the gradient is independent of the dimension of the design variables [32]. However, the gradient-based optimization method is a local optimization method, which can easily fall into local optimization; the optimization results often depend on the choice of the optimization starting point, which is not conducive for obtaining the global optimal solution.

To improve the aerodynamic shape design optimization, non-gradient optimization methods [33] are used for aerodynamic shape design optimization; for example, genetic algorithms [34,35], particle swarm algorithms [36], evolutionary differential algorithms [37], and simulated annealing [38]. Although these heuristic algorithms have global search properties, they require a large number of function evaluations to search for the global optimum. Currently, CFD has evolved to solve the Reynolds equation and the trapped and large vortex simulations, which are already time-consuming to perform a single CFD calculation. As can be imagined, it is expensive and unacceptable to use these heuristic algorithms to directly apply CFD for aerodynamic design. To balance the optimization efficiency and effectiveness of the aerodynamic shape design optimization, a hybrid optimization algorithm combining heuristic and gradient algorithms is used in optimizing the design to improve the efficiency and effectiveness of the optimization [39–41].

2.3. Evaluation of Aerodynamic Characteristics

As shown in Figure 1, an important function of the ASO framework is to accurately evaluate the aerodynamic characteristics of new shapes, including aerodynamic shape parameterization, aerodynamic mesh generation/deformation, and CFD simulation.

First, the aerodynamic shape can be changed by controlling the parameters of the aerodynamic shape parameterization methods, which significantly influence the optimal results of ASO. A good parametric method should have the ability to cover more potential shapes with fewer design parameters in the design space [42]. Various aerodynamic shape parametric methods have been developed and applied to ASO, such as the parametric section (PARSEC) method and its developed methods [43],Hicks–Henne function methods [44], class-shape function transformation (CST) methods [45], and free-form deformation methods [46,47]. In this study, we adopt a POD-based CST airfoil parametric method that was proposed in our previous study [48] for airfoil shape optimization. The detailed POD-based CST airfoil parameterization method is provided in Appendix A.1. The 3-D CST parameterization method is adopted in this study to parameterize the wing shape. The detailed 3-D CST wing parameterization is provided in Appendix A.2.

Second, the aerodynamic mesh must be regenerated or updated before evaluating the aerodynamic characteristics of the changed aerodynamic shape. That is, new aerodynamic meshes should be generated according to the new shapes in the optimization process. If a mesh generator is used to regenerate the new mesh, the optimization process will become time-consuming. To make the grid update easier, the space position of the aerodynamic grid can be changed based on the current grid with grid deformation techniques. For example, Jakobsson and Amoignon [49] developed a radial basis function (RBF)-based mesh deformation technology and applied it to ASO design. Poirier and Nadarajah [50] developed an efficient RBF-based mesh deformation method for an adjoint-based aerodynamic optimization framework. Furthermore, the RBF-based grid deformation method is adopted in the proposed framework.

Lastly, CFD simulations are used to evaluate the aerodynamic characteristics. We adopt a flow solver as the CFD tool for the aerodynamic characteristics evaluation. In the

flow solver, steady-state flow solutions are computed using the Reynolds-averaged Navier–Stokes equations along with the S-A turbulence model. Additionally, the cell-centered finite volume method is used for spatial discretization, and the AUSM+-up scheme is used to evaluate the numerical flux. The symmetric Gauss–Seidel iterative time-marching scheme is applied in the pseudo time step, and the second-order accurate full implicit scheme is used to solve the equations in the physical time step. Previous studies have used the flow solver for unsteady flows and aerodynamic design [51–53].

3. Construction of the Data-Driven Surrogate-Aided Aerodynamic Shape Optimization Framework Based on the TLBO Algorithm

As introduced in Section 2, the aerodynamic design optimization comprises geometric parameterization modules, automatic mesh generation, CFD simulations, and optimization methods. In this section, an aerodynamic data-driven surrogate-assisted teaching-learning-based optimization (TLBO) framework for constrained aerodynamic design is proposed. Figure 2 displays the flowchart of the proposed DDSAO framework for aerodynamic design. As shown in Figure 2, the TLBO algorithm is selected as the basic optimization algorithm due to its parameter-free adjustment characteristics and strong optimization ability. DO with TLBO is the basic component in the proposed framework. In the DO component, the TLBO algorithm is used to directly optimize the CFD for aerodynamic design optimization.

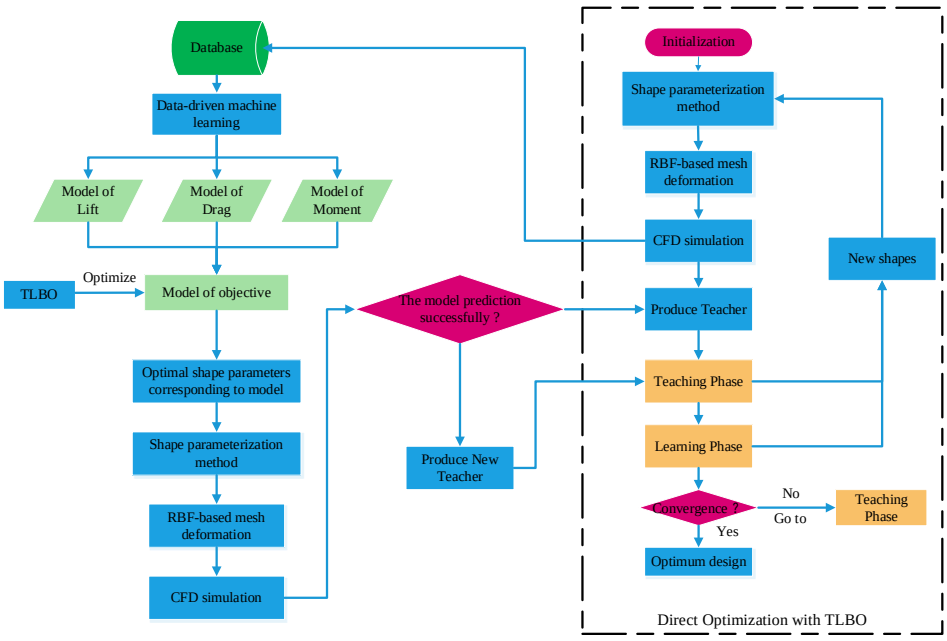

Figure 2. Flowchart of the data-driven surrogate-assisted optimization framework for aerodynamic design.

Moreover, Figure 2 shows that historical aerodynamic data are generated when the real CFD simulations are conducted, which are used to evaluate the aerodynamic characteristics of new airfoil shapes during the aerodynamic optimization process with the TLBO algorithm. In this study, we attempt to mine useful information from these historical aerodynamic data to guide and accelerate the aerodynamic optimization process. Using the knowledge and information contained in the aerodynamic data, DO with TLBO is supported via an adaptive data-driven surrogate-assisted support strategy. The detailed introduction is as follows.

3.1. Direct Optimization with TLBO Algorithm

The TLBO algorithm is a type of heuristic algorithm based on a pattern of "teaching" and "learning" [25]. The TLBO algorithm uses a concept of "knowledge level," representing

the objective function value of population individuals. The population individuals contain the teacher and students. The teacher is the best individual in the population. TLBO aims to improve the knowledge level of the all-population individuals by both teaching and learning phases. In the teaching phase, the students improve their knowledge level based on the teacher's guidance. In the learning phase, the students improve their knowledge via mutual discussion. During the TLBO optimization process, the teaching and learning phases are repeated generation by generation until the optimal value is found. The detailed TLBO algorithm is provided in Appendix B.

As shown in Figure 2, the TLBO algorithm is used to directly optimize the CFD for ASO. The DO framework includes aerodynamic shape parameterization, computational grid deformation, CFD simulation, and the TLBO algorithm. This DO with TLBO is the basic component of the proposed framework. According to the introduction of the TLBO algorithm, new individuals are continuously generated from the teaching phase [Equations (A15) and (A16)] and learning phase [Equation (A19)] during the TLBO optimization process. These new individuals must be aerodynamically evaluated using CFD. Thus, the aerodynamic data that characterize the relation between shape and aerodynamic characteristics are continuously generated during the TLBO optimization process.

These aerodynamic data contain considerable useful information and knowledge that can be beneficial for the aerodynamic optimization search. However, most of them are underutilized in the DO framework because the individuals that fail in the competitive selection are abandoned and no longer reused in the following optimization process. Therefore, "data-driven" denotes the full utilization of the information and knowledge contained in these aerodynamic data for effectively guiding the optimization process. We use the aerodynamic data generated during the TLBO optimization process to assist in the aerodynamic optimization search. To effectively use these aerodynamic data to support the ASO, an adaptive data-driven surrogate-assisted support strategy is proposed.

3.2. Adaptive Data-Driven Surrogate-Aided Support Strategy

Figure 2 shows that the proposed adaptive data-driven surrogate-assisted support strategy mainly includes data-driven surrogate model learning and the surrogate-assisted support strategy.

In data-driven surrogate model learning, a surrogate model is constructed according to the aerodynamic data generated in the optimization process. First, a relevant surrogate model, such as Kriging, RBF neural network, or support vector machine, is selected according to the requirements. The Kriging model has been widely used as a surrogate model due to its good nonlinear fitting ability [54,55]. It is also adopted in this study. The principle and formula derivation of Kriging model are given in Appendix D.

Then, an online model learning strategy is used as the model management strategy. Since the aerodynamic data are generated and stored generation by generation, the surrogate model is adaptively updated by the supplementary data based on the online model learning strategy. The generation-based online model management strategy is adopted herein.

Based on the TLBO algorithm structure, the model optimal prediction (MOP) method is proposed as the surrogate-assisted support strategy. That is, the surrogate models are used to predict the knowledge of the teacher via MOP. The MOP steps are as follows:

Step 1: After the surrogate models process the aerodynamic data, the penalty function method is used to convert the constrained optimization to an unconstrained optimization, following Equation (2).

Step 2: An optimization algorithm (TLBO is used herein) is selected to optimize the converted objective. Optimal individuals corresponding to the aerodynamic models can be obtained. The optimal individual is set as X^(T,MOP).

Step 3: X^(T,MOP) must be compared with the teacher (X^T) of the current generation to determine whether it can be used for the teaching phase. A new individual is evaluated by real CFD simulation. The drag, lift, and moment coefficients are obtained through

CFD simulations, and the objective function value F (X^(T,MOP)) is determined using Equation (2).

Step 4: It is determined whether the MOP is successful. If F (X^(T,MOP)) < F (X^T), the teacher by MOP replaces the current teacher. Otherwise, the current teacher X^T remains.

Step 5: Then, the new teacher produces new individuals through the teaching phase.

3.3. Validation and Verification

Before the proposed optimization method is applied to aerodynamic design, a one-dimensional Rastrigin function is used to demonstrate the data-driven optimization process of the proposed algorithm. The population size (N_p) is set as 5. Figure 3 displays the data-driven optimization process of the one-dimensional Rastrigin function. The figure presents the distribution of these incremental data generated during the optimization process. With increasing data, the difference between the data-driven learning model and the real function gradually decreases. The data-driven learning model can accurately predict that the minimum value of the Rastrigin function at generation is 4. Through the simple example, it can directly reflect the principle of accelerating the TLBO optimization process by fully utilizing the historical process data of the data-driven TLBO algorithm.

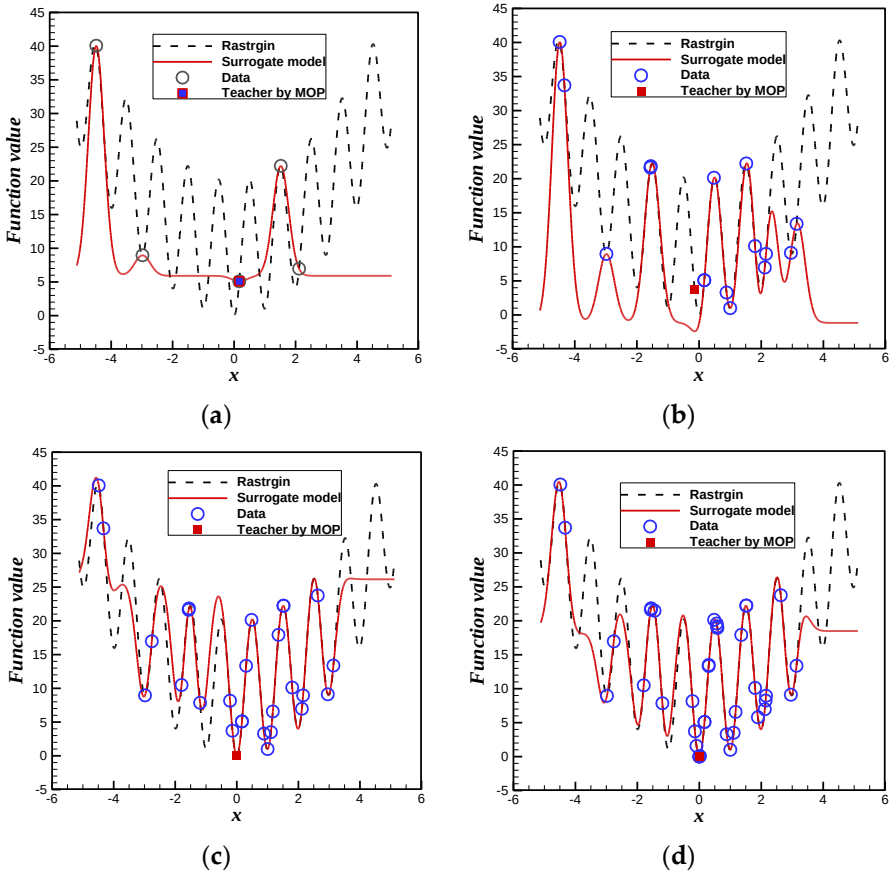

Figure 3. Demonstration of the data-driven optimization process using the one-dimensional Rastrigin function. (**a**) Generation = 1; (**b**) Generation = 2; (**c**) Generation = 3; (**d**) Generation = 4.

4. Benchmark Aerodynamic Design Optimization for Drag Minimization of RAE2822 Airfoil in Transonic Viscous Flow

4.1. Benchmark Aerodynamic Shape Optimization Problem Statement

The benchmark ASO for the drag minimization of the RAE2822 airfoil in the transonic viscous flow is provided by the aerodynamic design optimization discussion group

(ADODG) of AIAA in this study [56–62]. The design state is Ma = 0.734 and Re = 6.5 × 10^6. The mathematical description of the optimization problem is as follows:

$$\begin{gathered} Min\ C_d \\ S.t.\ C_l = 0.824 \\ C_m \geq -0.092 \\ A \geq A_{initial} \end{gathered} \tag{3}$$

where C_l, C_d, and C_m are the lift, drag, and pitching moment coefficients, respectively. A denotes the area of the optimized airfoil, and $A_{initial}$ denotes the area of the initial airfoil.

The grid convergence study for the initial RAE822 airfoil is conducted before the beginning of the aerodynamic design optimization. Table 1 shows the convergence of the aerodynamic coefficients for different grid sizes. The difference in C_l of RAE2822 converges within 0.1 counts and that in C_d converges within 1.0 counts with the gradual increase of cells. The computational grid is shown in Figure 4, and the grid size of 256 × 120 is used in this study.

Table 1. Grid convergence study of aerodynamic performance for RAE2822.

Grid Size	Cl	Cd (Counts)
128 × 64	0.823	208.6
192 × 96	0.824	202.3
256 × 120	0.824	195.3
320 × 160	0.824	194.9
448 × 256	0.824	194.8

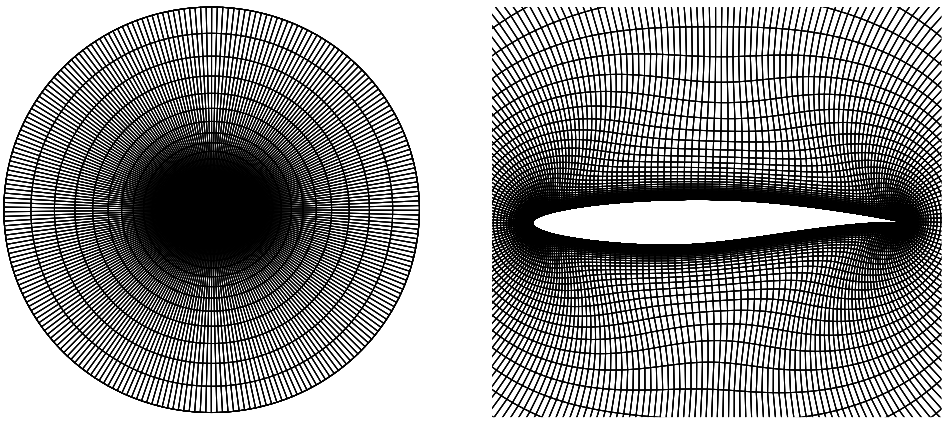

(**a**) (**b**)

Figure 4. Computational grid of the airfoil RAE2822. (**a**) Global grid; (**b**) Local grid.

4.2. Drag Minimization of RAE2822 Airfoil in Transonic Viscous Flow

In this section, the proposed method is used in the benchmark ASO for the transonic drag minimization of the RAE2822 airfoil. Additionally, relevant comparisons of the optimization results are conducted to verify the superiority of the proposed method. The comparative study is conducted from two aspects. First, the DDSAO framework results are compared with the results of the DO framework with TLBO, DE, and PSO algorithms to verify the efficiency, effectiveness, and nonparametric characteristics of the proposed method. Second, the optimization results are compared with other benchmark results to verify the optimization ability of the proposed method.

For these optimization algorithms, the population number (N_p) parameter is set. The number of function evaluations of each generation for the TLBO algorithm is twice that

of N_p. For the proposed framework, the number of CFD evaluations for each generation is $2N_p + 1$. For the DE and PSO algorithms, the number of function evaluations for each generation is N_p. The parameter N_p of TLBO and DDSAO is set as 10, and those of the DE and PSO algorithms are set as 20. Moreover, these different algorithms perform 10 independent operations on each test problem to obtain the robust optimal results.

In addition to N_p, other optimization parameters must be adjusted in the DE and PSO algorithm frameworks. The parameter mutation rate (MR) and crossover rate (CR) must be set up in the optimization process for the DE algorithm. The parameter inertia weight (w) and learning factors (c_1 and c_2) must be set up for the PSO algorithm. Two groups of parameters of PSO and DE algorithms are randomly selected for comparison in this study to illustrate the influence of different parameter settings on the optimization results. Parameters MR and CR of the DE algorithm are selected as (0.4, 0.5) and (0.6, 0.8), respectively; and w, c_1, and c_2 are set as (0.3, 1, 1) and (0.5, 2, 2), respectively.

The optimization efficiency and effect of the proposed method are compared with those of the DO framework with TLBO, DE, and PSO algorithms as the basic optimizer. Figure 5 shows the convergence process and reduction of C_d with information generation for the different ASO methods. The calculation results are the average of 10 independent operations of different algorithms on each test problem. Figure 5a displays the average iteration process of these optimization algorithms with the optimization process. Compared to the other methods, the proposed method significantly improves the optimization efficiency. Furthermore, based on the optimization ability, the proposed method yields better optimal results with fewer CFD evaluations than the other methods. Figure 5b shows the reduction of C_d with the generation evolutionary process. The proposed method can reduce C_d 40% faster than the other methods, validating its effectiveness. Lastly, Figure 5 shows that the different optimization parameters considerably influence the convergence processes and optimization abilities of the DE and PSO algorithms, which will inevitably increase the complexity of engineering optimization for designers. The proposed method, which is developed from the nonparametric TLBO algorithm, can avoid the disadvantages of parameter adjustment. Figure 6 provides the error bars of the drag coefficient with the convergence process for the different ASO methods. The small error bars indicate that the difference between independent runs is small. Thus, the convergence of error bars shown in Figure 6 can reflect the convergence stability of the different methods. Moreover, the fluctuation of the optimized C_d by the proposed method is much smaller than that by other methods. This indicates that the proposed method is beneficial for the convergence of optimization via data-driven learning method.

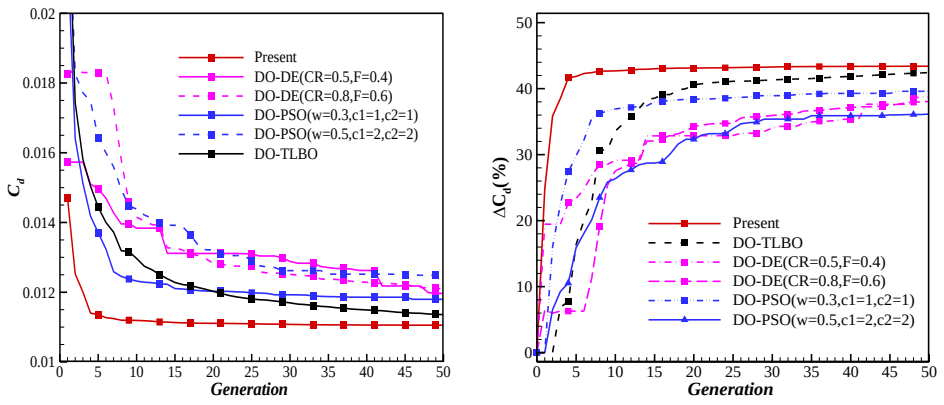

(**a**) (**b**)

Figure 5. Convergence process and reduction of drag coefficient (C_d) with the generation process by different ASO methods. (**a**) Average convergence process of C_d; (**b**) Reduction of C_d.

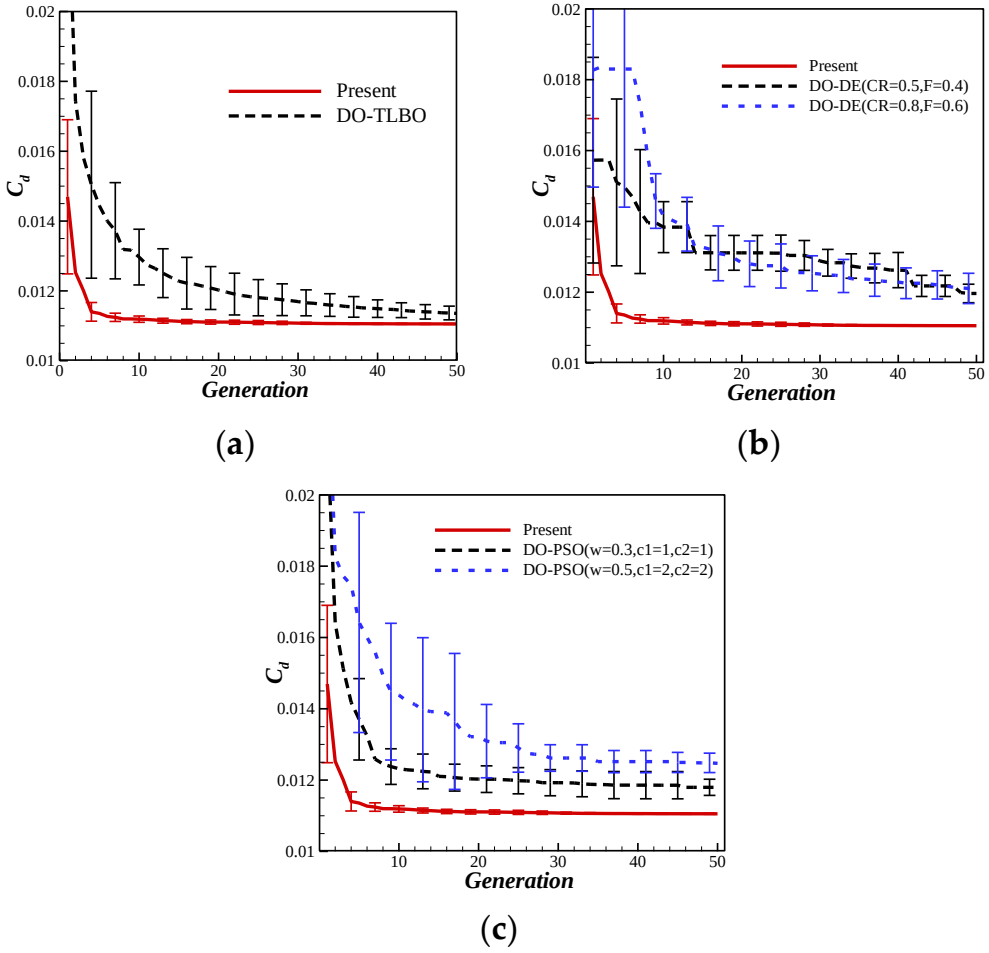

Figure 6. Error bar of the drag coefficient (C_d) with the convergence process. (**a**) Present (DDSAO-TLBO) vs. DO-TLBO; (**b**) Present vs. DO-DE; (**c**) Present vs. DO-PSO.

Additionally, the C_p contour with the optimization process should be analyzed. We compare the C_p contour of the optimal airfoil at generations of 5, 10, 20, 30, and 40. Figure 7 shows the variation of the C_p contour with increasing generation by different methods. The proposed method reduces the shock intensity faster than the other methods. Furthermore, the shock intensity of the proposed method at G = 5 is even smaller than that of other methods at G = 40. The C_p contour changes show that different parameter settings significantly affect the optimization results of the DE and PSO algorithms, reflecting the benefits of the nonparameter adjustment of the TLBO algorithm. Figure 8 shows the comparisons of C_p and airfoil shapes with the optimized airfoils. The optimized airfoil shape and corresponding C_p by the present method at G = 5 are compared with those by other SAO methods at G = 40. The shock wave intensity of the optimized airfoil by the present method is obviously smaller than that by other methods. Moreover, the location of the maximum thickness of the optimized airfoil moves rearward, similarly to other SAO methods, which can explain the reason for the weaker shock strength.

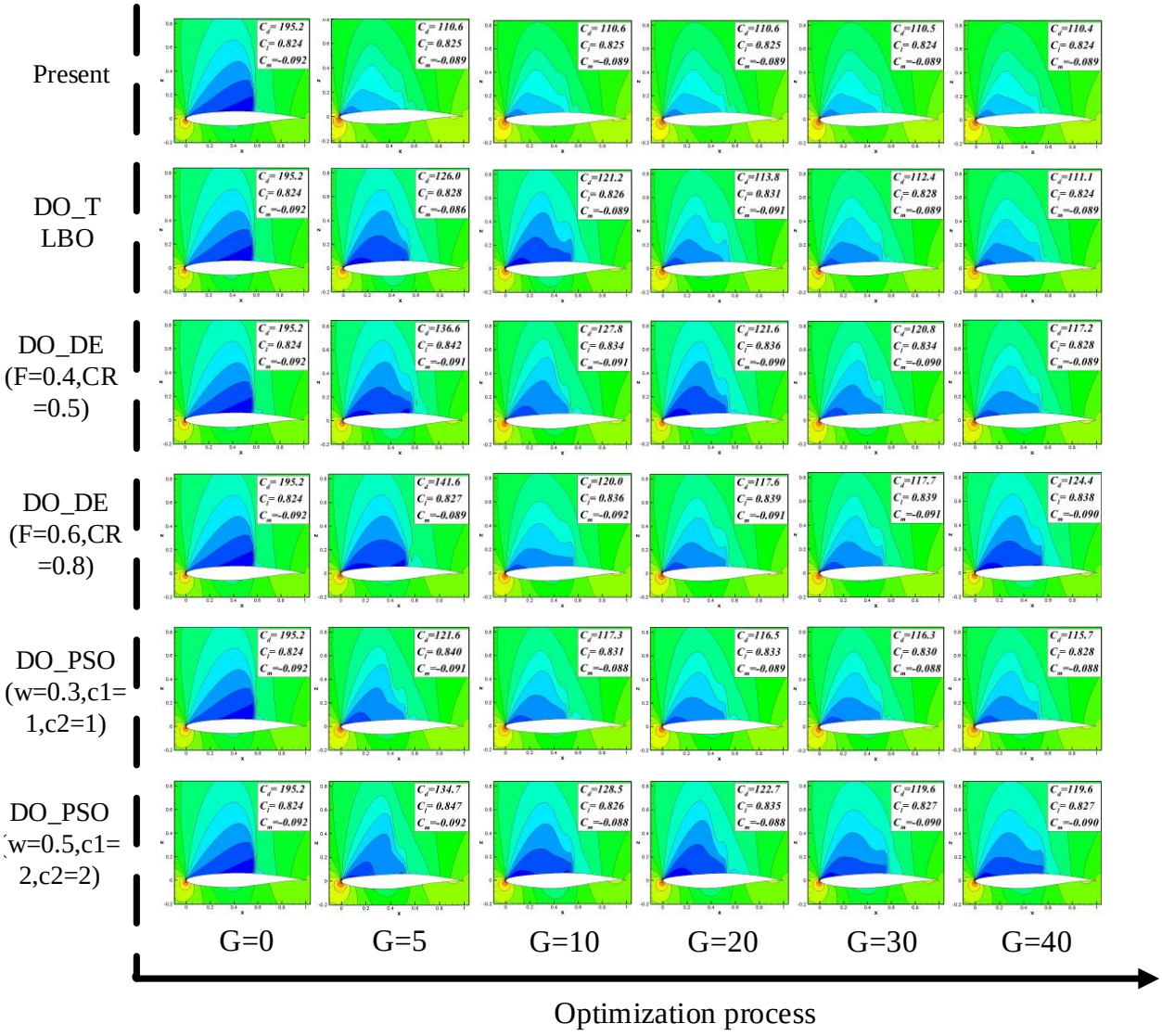

Figure 7. C_p Contour convergence with the optimization process.

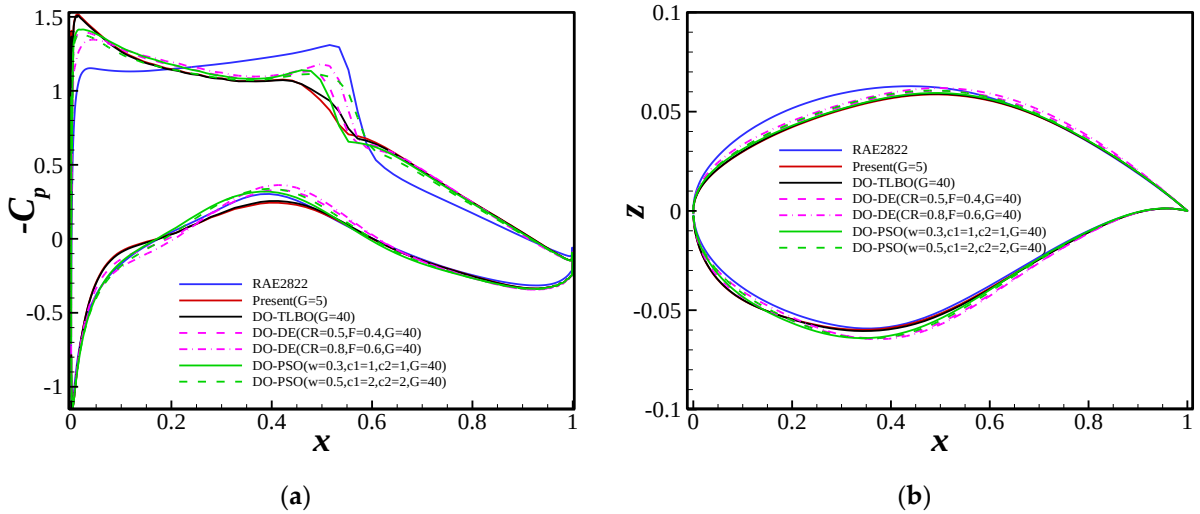

(**a**) (**b**)

Figure 8. Comparisons of C_p and airfoil shapes with the optimized airfoils. (**a**) C_p distribution; (**b**) airfoil shapes.

Therefore, the comparison of the benchmark ASO examples shows that the proposed algorithm has more powerful optimization ability than the common heuristic algorithms and it can maintain the nonparametric characteristic. Notably, the advantages of the proposed method are reflected in the optimization efficiency, optimization effect, and parameter-free adjustment characteristics.

The benchmark ASO for drag minimization of the RAE2822 airfoil in the transonic viscous flow is provided by ADODG of AIAA. Many international counterparts in the field of ASO have also studied the benchmark case [56–62]. However, due to the use of different solvers, numerical formats, and mesh sizes, it is not recommended to directly compare the optimization results with them. To highlight the excellence of this method and avoid unfair comparison, we used different optimization methods for the same case, including gradient methods and different heuristic algorithms.

As shown in Figure 8, the shock wave intensity of the proposed method is obviously weaker than that of other optimized results. We also perform the gradient-based optimization. The reduction of C_d by gradient-based optimization is about 30%, while that by the proposed method is 43%. Therefore, the optimization effect of the proposed method is verified.

5. Aerodynamic Shape Optimization for 3-D Wing Shape Design

5.1. Aerodynamic Shape Optimization Problem Statement of the 3-D Wing

First, the mathematical optimization model is constructed. The objective function, constraint function, and design variables for ASO are determined according to the specific engineering requirements. The optimization is conducted considering the drag reduction of the wing under geometric and lift constraints. The specific mathematical optimization model is as follows:

$$\begin{gathered} Min\ C_d \\ s.t.\ C_l \geq C_{l0} \\ V \geq V_{initial} \\ \boldsymbol{x_L} \leq \boldsymbol{x} \leq \boldsymbol{x_U} \end{gathered} \tag{4}$$

Here, C_d is the resistance coefficient; C_l is the lift coefficient; V is the volume of the wing; and $\boldsymbol{x_L}$ and $\boldsymbol{x_U}$ represent the lower and upper bounds of the design variables, respectively.

Then, the wing used for ASO is introduced. The geometric plane parameters of the wing are as follows: root chord length is c = 1, wing span is b = 1.5, swept-back wing is $\Lambda = 30^\circ$, and taper ratio is $\Gamma = 0.5$. The wing cross-sectional shape is the NACA0012 airfoil. The nonstructural mesh is employed as the computational grid, as shown in Figure 9. The design state is selected at the transonic condition of Ma = 0.83, $\alpha = 3.06^\circ$, and Re = 6.5×10^6.

Table 2 shows the convergence of the drag coefficients for different grid sizes. With the increase of the number of grids, the drag coefficient changes by about 2%. This error is acceptable for the wing example. Due to the large amount of calculation of the wing example, we selected a relatively sparse grid of 271,404 cells for this study.

Table 2. Grid convergence study of aerodynamic performance for a 3-D wing.

Grid	Number of Cells	C_d (Counts)
1	271,404	436.0
2	678,282	436.1
3	1,054,179	425.3
4	1,571,430	427.5

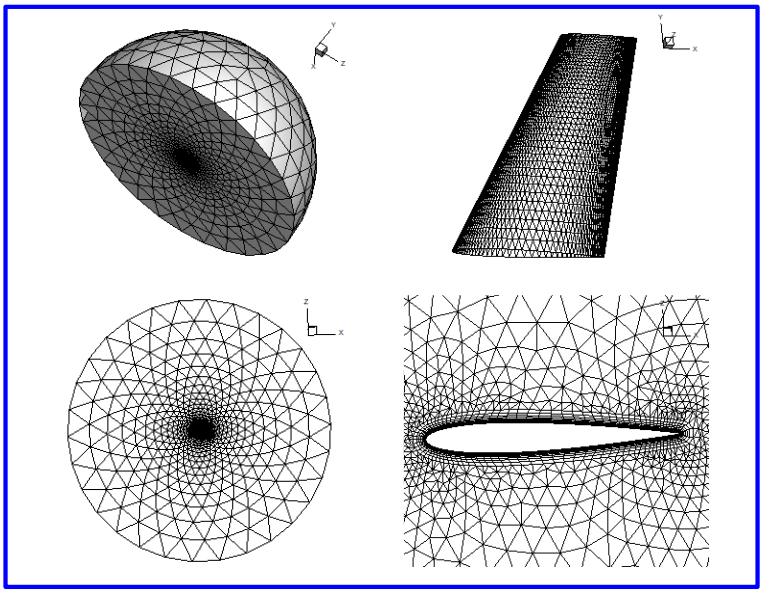

Figure 9. Computational grid of 3-D wing.

5.2. Aerodynamic Shape Optimization of a 3-D Wing

To verify the superiority of the proposed DDSAO-TLBO method for the 3-D wing shape design, the SBO and DO frameworks are applied for the wing shape design. The detailed DO and SBO frameworks are presented in Appendix C.

The DDSAO and DO frameworks employ the TLBO algorithm as the basic optimizer, and they both employ N_p as the optimization parameter. In this study, the N_p of TLBO and DDSAO is set as 10. According to Appendix C, the employed SBO is an adaptive SBO framework. Two hundred sample points are selected as initial points to construct the initial surrogate model, and the surrogate model is updated by the infilling strategy. We adopt an infilling strategy wherein the optimal design point is added to update the surrogate model.

To maintain the fairness of comparison, we compared the convergence of the drag coefficient with the number of CFD evaluations. The number of CFD evaluations represents the efficiency of various methods. Figure 10 displays the convergence process of C_d with the number of CFD simulations by the DO, SBO, and DDSAO methods. The proposed DDSAO method considerably improves the optimization efficiency compared to the other methods. Furthermore, the proposed method yields better optimal results, with fewer CFD evaluations than the SBO and DO frameworks from the optimization ability perspective.

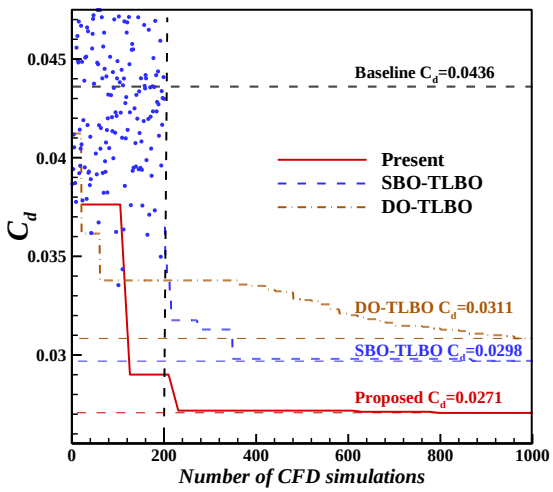

Figure 10. Convergence process drag coefficient (C_d) by proposed, SBO, and DO methods.

Moreover, the pressure coefficient (C_p) distributions and airfoil shapes of the different sections are compared to verify the optimization effect of the proposed method. Figure 11 presents the comparisons of C_p and shape for the different sections of the airfoil by the three ASO methods. The shock wave intensity of the optimized airfoil by the proposed method is obviously smaller than that by the other methods. Additionally, for the proposed method, the location of the maximum thickness of the optimized airfoil moves rearward, compared to that for the other SAO methods, which explains the reason for the weaker shock strength. The wing surface pressure contours are shown in Figure 12. The proposed method successfully weakens or eliminates the shock wave of the wing surface, which is the main driver for reducing the drag. These comparisons of the 3-D wing shape optimization design show that the optimization efficiency and optimization effect of the proposed method is significantly better than those of the SBO and DO frameworks.

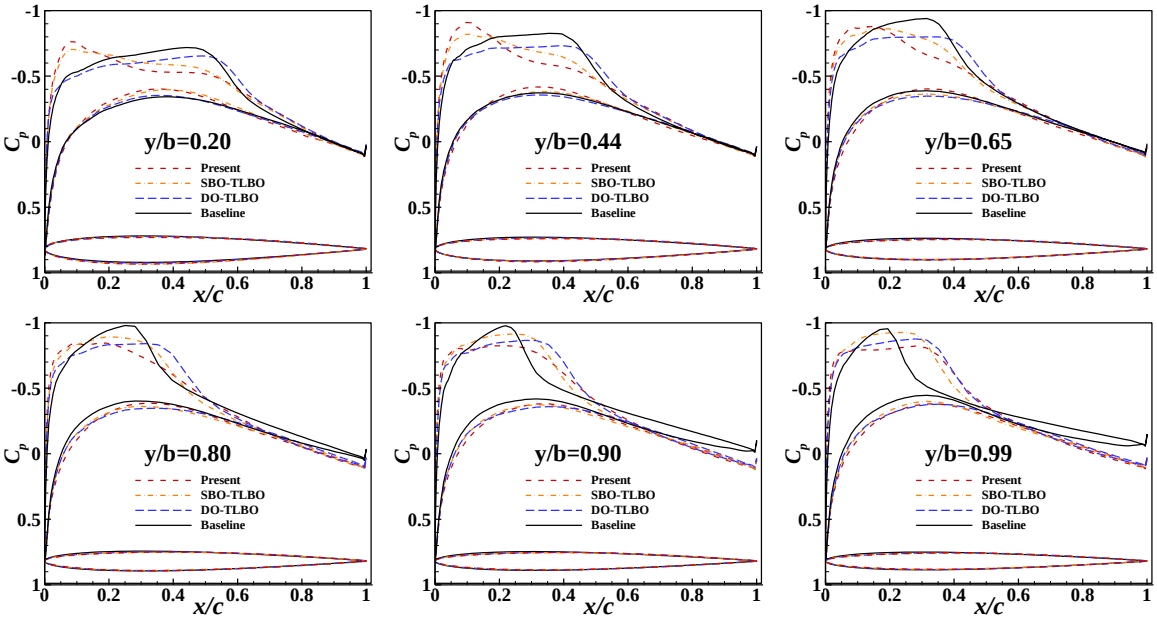

Figure 11. Comparisons of C_p and shape with the different sectional airfoils.

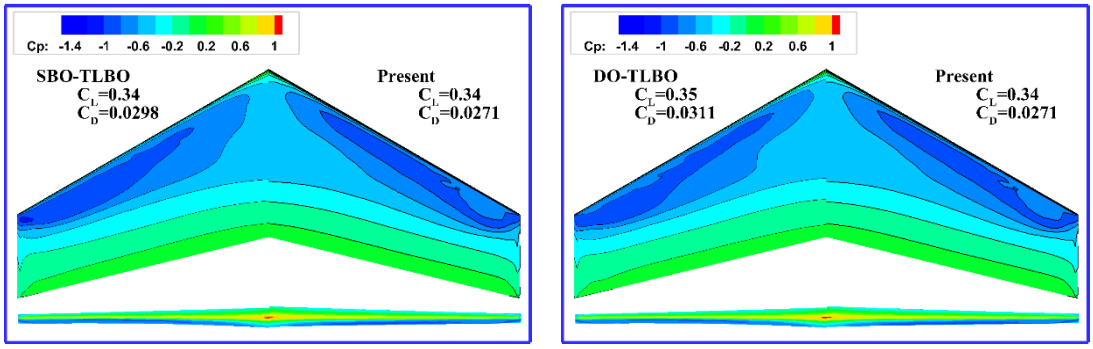

Figure 12. Surface pressure contours of a wing by present, DO, and SBO frameworks.

6. Conclusions

To fully utilize the historical aerodynamic data generated during the gradient-free optimization process and reduce the influence of optimization parameters adjustment on the ASO result as much as possible, the study proposed an aerodynamic data-driven surrogate-assisted aerodynamic shape optimization framework using a teaching-learning-based TLBO algorithm for aerodynamic designs. The proposed ASO method was applied to the aerodynamic design of an airfoil and a wing. First, the benchmark ASO was applied for the drag minimization of the RAE2822 airfoil in a transonic viscous flow. The comparison

of the results from different ASO frameworks showed that the proposed framework can considerably improve the efficiency compared to the DO framework. Furthermore, it has nonparametric characteristics, which is convenient for engineering applications. Moreover, the obtained optimization results were compared with those of international counterparts of ASO. The proposed method yielded better optimization performances than the international counterparts. Second, the proposed method was applied to 3-D wing shape optimization design. The optimization results showed the advantage of the proposed method over the SBO and DO frameworks. Therefore, the proposed method can effectively gain knowledge from the historical process data to guide the ASO search process.

Author Contributions: Conceptualization, X.W. and Z.Z.; methodology, L.M.; software, X.W.; validation, X.W., Z.Z. and L.M.; formal analysis, X.W.; investigation, Z.Z.; resources, X.W.; data curation, L.M.; writing—original draft preparation, X.W.; writing—review and editing, L.M.; visualization, Z.Z.; supervision, X.W.; project administration, X.W.; funding acquisition, X.W. All authors have read and agreed to the published version of the manuscript.

Funding: This research was funded by the National Natural Science Foundation of China Youth Fund (No. 11902235), the China Postdoctoral Science Foundation (2018M643588), the Basic Research Programs of Taicang (TC2020JC14), the Fundamental Research Foundation for the Central Universities (D5000210513), Double First-Class University Construction Foundation of China (0638021GH020116), and the Natural Science Foundation of Shaanxi Province (2021JQ-081).

Data Availability Statement: Not applicable.

Conflicts of Interest: The authors declare no conflict of interest.

Appendix A. The Introduction of the CST-POD-Based Airfoil Parameterization and 3-D CST Parameterization of the Wing

Appendix A.1. CST-POD Based Airfoil Parameterization

The Class-Shape Function Transformation (CST) is an airfoil parametric method proposed by Kulfan and Bussoletti which represents a two-dimensional geometry by the product of a class function C(x/c) and a shape function S(x/c) plus a term that characterizes the trailing edge thickness:

$$\frac{y}{c} = C\left(\frac{x}{c}\right)S\left(\frac{x}{c}\right) + \frac{x}{c}\frac{\Delta Z_{te}}{c} \tag{A1}$$

where C(x/c) is given in generic form by:

$$C\left(\frac{X}{C}\right) = \left(\frac{X}{C}\right)^{N_1}\left(1-\frac{x}{c}\right)^{N_2} 0 \le \frac{x}{c} \le 1 \tag{A2}$$

The exponents N_1 and N_2 define the type of geometry to be represented. An airfoil, for example, is represented by $N_1 = 0.5, N_2 = 1$.

The shape function is defined on the basis of Bernstein binomials, by the introduction of weight factor b_i as follows:

$$S\left(\frac{x}{c}\right) = \sum_{i=0}^{n}\left[b_i \cdot \frac{n!}{i!(n-i)!}\left(\frac{x}{c}\right)^i\left(1-\frac{x}{c}\right)^{n-i}\right] \tag{A3}$$

Taking NACA0012 airfoil as an example to verify the fitting ability of CST, Figure A1 gives the geometric representation and error analysis by CST method. It can be observed that the fitting ability of CST is very good.

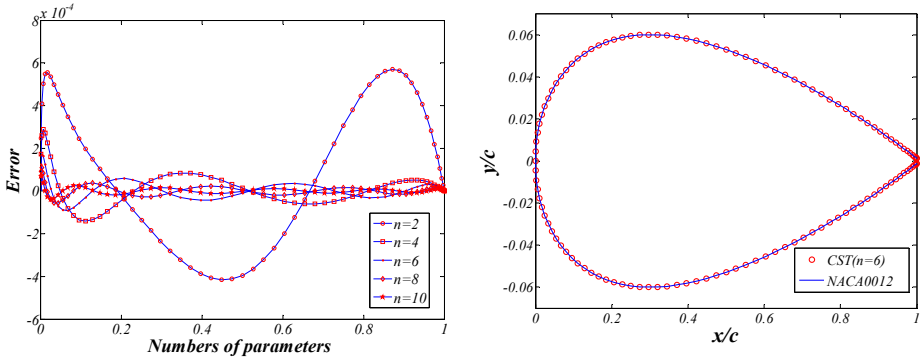

(**a**) (**b**)

Figure A1. Geometric representation and error analysis. (**a**). The error with the number of parameters; (**b**). Airfoil parameterized by six design variables.

The POD with high-dimensional CST parametric methods is combined to construct a new POD-based CST parametric method. Firstly, an existing high-dimensional parametric method is used to describe the airfoil shape. A series of geometric shapes are obtained by randomly changing the parameters as the sampling snapshots in the selected design space. The snapshots matrix S is represented as:

$$S = [s_1, s_2, \ldots, s_N] \tag{A4}$$

Then, the POD analysis is conducted to get a set of orthogonal POD basis functions. The average vector $\bar{\mathbf{s}}$ of the snapshots is:

$$\bar{\mathbf{s}} = \frac{1}{\mathbf{N}} \sum_{i=1}^{N} s_i \tag{A5}$$

By defining $X = S - \bar{\mathbf{s}}$, the correlation matrix is constructed as follows:

$$\mathbf{R} = \mathbf{X}^{\mathrm{T}}\mathbf{X} \tag{A6}$$

The eigenvalue analysis of $\mathbf{R}$ is carried out to obtain corresponding eigenvalues λ and eigenvectors v. The eigenvalue determines the importance of the snapshot information contained in the POD basis functions. Usually, the first few POD basis functions contain more than 90% data information. The airfoil geometry can be expressed as:

$$\mathbf{s} = \bar{\mathbf{s}} + \sum_{\mathrm{i}=1}^{\mathrm{n}} \alpha_i \mathrm{v}_i \tag{A7}$$

It can be observed that the airfoil shapes are represented through the change of parameter α_i. In this way, the geometric shapes of airfoils can be described by using the first few important POD basis functions, which can greatly reduce the number of design variables to describe the variations of airfoil shapes. Meanwhile, the ability to cover potential optimized shapes is maintained at the same level as the original high-dimensional parametric method.

Taking the upper surface of NACA0012 airfoil as an example, 12 CST parameters are used to describe the airfoil geometry shape. CST parameters are changed to obtain a series of airfoil shapes as sample snapshots. Through the POD analysis, a series of reduced POD orthogonal basis functions are obtained to describe the variations in airfoil shape. Figure A2 shows the eigenvalues varying with the number of POD modes. It is observed that the proportion of the first six modes is 98.32%, which indicates that the first six POD basis functions can almost reach the same ability to describe the variation as the CST method with 12 parameters has. Moreover, 10 test airfoils are randomly selected in the

design space to carry out the fitting error analysis. Figure A3 shows shapes of test airfoils and corresponding fitting errors with the number of POD modes. It can be observed that the fitting errors have been greatly reduced when the modal order reaches more than six. Figure A4 shows the distribution of the first six POD basis functions of the airfoil upper surface, which are in a sinusoidal curve form. The number of peaks contained in the POD basis increases with the modal order. As is shown in Figure A2, the high order POD basis is gradually becoming less important with the increase of order in describing the airfoil. Therefore, we believe that the first few modes are sufficient to describe the variations in airfoil shape. Figure A4 shows the deformation of the first six deformation modes of the airfoil upper surface. It can be observed that these geometric modes are global geometric deformation modes and present some typical geometric deformation. Specifically, mode 1 is the scale mode in the thickness direction; mode 2 is the translation mode of the maximum thickness in the axial direction; and modes 3–6 are the extrusion modes of the upper surface.

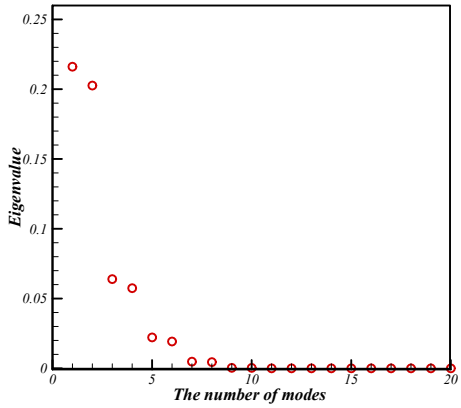

Figure A2. The eigenvalues with the number of modes (NACA0012, 12 CST).

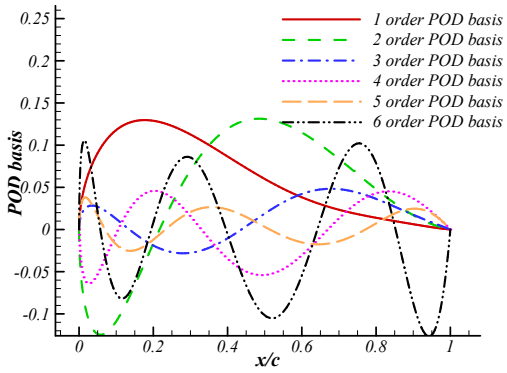

Figure A3. The first six POD basis functions of the upper surface of airfoil.

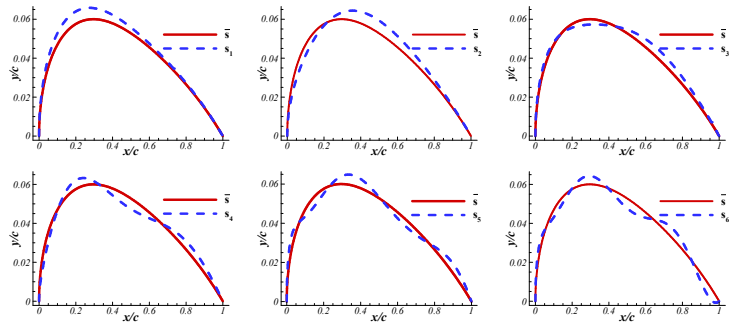

Figure A4. The deformation of the first six POD modes of the airfoil upper surface.

Appendix A.2. 3-D CST Parameterization Method

The three-dimensional CST method can be regarded as a distribution of two-dimensional airfoils across the span direction. Equation (A8) can be used to obtain analytical formulations of the wing airfoil sections. Then, these airfoils can be interpolated across the span to define the whole wing. The Bernstein polynomials can be used as the interpolation functions along span direction in three-dimensional parameterization. Those shape functions of the three-dimensional CST method can be expressed as:

$$S(\psi,\eta) = \sum_{i=0}^{n}\sum_{j=0}^{m} b_{i,j} B_n^i(\psi) B_m^j(\eta) \tag{A8}$$

$B_n^i(\psi)$ is the chordwise Bernstein function and $B_m^j(\eta)$ is the spanwise Bernstein function. The expressions are shown in Equations (A9) and (A10):

$$B_n^i(\psi) = \frac{n!}{i!(n-i)!} \cdot (\psi)^i (1-\psi)^{n-i} \tag{A9}$$

$$B_m^j(\eta) = \frac{m!}{j!(m-j)!} \eta^j (1-\eta)^{m-j} \tag{A10}$$

where ψ and η represent the nondimensional coordinate values of the chord and span directions of the wing, respectively. The coefficients $b_{i,j}$ represent the weights of the different analytical formulations. The formulation for the number of $b_{i,j}$ is as follows:

$$Num_{b_{i,j}} = (n+1)\cdot(m+1) \tag{A11}$$

where n is the order of the chord and m is the order of the span. The different wings are parameterized by controlling the number and value of $b_{i,j}$.

Consequently, the geometry of the wing upper and lower surfaces can be expressed as:

$$\xi_U(\psi,\eta) = C_{N_2}^{N_1}(\psi) \sum_{i=0}^{n}\sum_{j=0}^{m} b_{U_{i,j}} \left[\frac{n!}{i!(n-i)!} \cdot (\psi)^i (1-\psi)^{n-i}\right] \left[\frac{m!}{j!(m-j)!} \eta^j (1-\eta)^{m-j}\right] \tag{A12}$$

$$\xi_L(\psi,\eta) = C_{N_2}^{N_1}(\psi) \sum_{i=0}^{n}\sum_{j=0}^{m} b_{L_{i,j}} \left[\frac{n!}{i!(n-i)!} \cdot (\psi)^i (1-\psi)^{n-i}\right] \left[\frac{m!}{j!(m-j)!} \eta^j (1-\eta)^{m-j}\right] \tag{A13}$$

where the coefficients $b_{U_{i,j}}$ and $b_{L_{i,j}}$ define the geometry of the wing upper and lower surfaces. The class function $C_{N_2}^{N_1}(\psi)$ is constructed by Equation (A2). Various wing planes can be obtained by controlling the wing plane parameters. In this paper, the class function $C_{N_2}^{N_1}(\psi)$ defines N_1 = 0.5, N_2 = 1 and the shape functions $\sum_{i=0}^{n}\sum_{j=0}^{m} b_{i,j} B_n^i(\psi) B_m^j(\eta)$ are shown as the Figure 3. The coefficients n and m of the upper and lower surfaces are 3 and 5, respectively.

The product of the class function and the shape function can be parameterized for three-dimensional wings. The complete construction of three-dimensional CST parameterization is shown in Figure A5. The parametric process for different types of wings is realized by changing the value of the $b_{i,j}$. The various wing planforms can be obtained by taper ratio, aspect ratio, and so on. Increasing the order of the chord and spanwise of the Bernstein polynomial can improve the fitting accuracy of three-dimensional CST parameterization and have a stronger ability to describe the potential aerodynamic shape in the design space. However, it will increase the difficulty of optimization and cause high-dimensional aerodynamic optimization design problems.

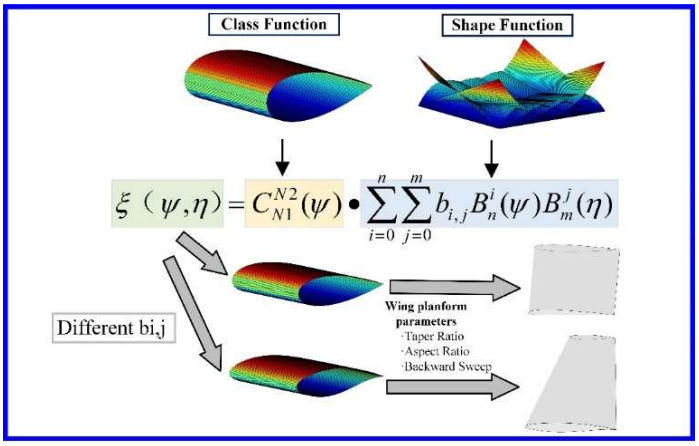

Figure A5. Three-dimensional CST parameterization process.

According to Equation (A11), the number of design variables is determined by parameters n and m. Figure A6 shows the wing fitting corresponding to different parameters. From the comparison of thickness contours, it can be observed that the fitting accuracy is improved with the increase of the number of design variables. The three-dimensional CST method can fit the original wing well at parameters $n = 4$, $m = 2$. Moreover, the fitting effects of different wing sections are further compared in Figure A7. The results demonstrated that the profiles of the different wing sections can fit well with original wing profiles when $n = 5$ and $m = 3$.

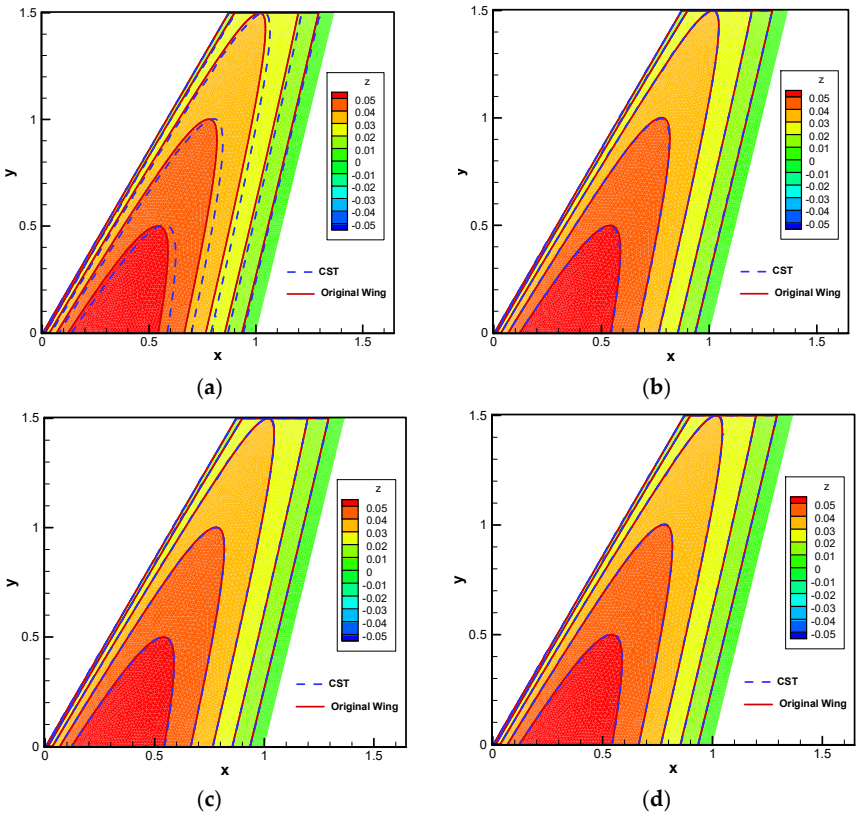

Figure A6. Fitting effect contours of the CST parameterization method; (**a**) n = 1, m = 2 ($Num_{b_{i,j}} = 6$); (**b**) $n = 2$, $m = 2$ ($Num_{b_{i,j}} = 9$); (**c**) $n = 4$, $m = 2$ ($Num_{b_{i,j}} = 15$); (**d**) $n = 5$, $m = 3$ ($Num_{b_{i,j}} = 24$).

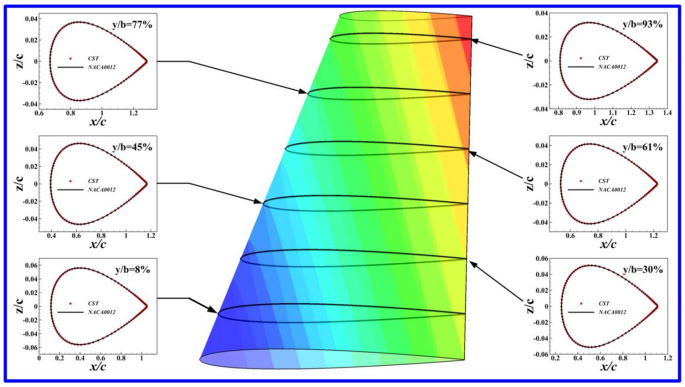

Figure A7. The fitting effect of the CST parameterization method for wing (n = 5, m = 3).

Appendix B. The Introduction of the TLBO Algorithm

The TLBO algorithm is a kind of heuristic algorithm based on the pattern of 'teaching' and 'learning'. TLBO shows good performance for complex optimization problems due to its simple implementation and strong optimization ability. A concept of 'knowledge level', which means the function value of a student or a teacher, is defined in the TLBO algorithm. $X^{teacher}$ represents the individual that has the highest knowledge level. In other words, the real function value of $X^{teacher}$ is greater than other students. The main idea of TLBO is to improve the knowledge level of both teacher and students by two phases. The first one is the teaching phase. The students must improve their knowledge level by the teacher's guidance in this phase. The second is the learning phase. The students improve their knowledge by mutual discussion in this phase. The best student after the learning phase will become $X^{teacher}$. Figure A8 shows the framework of the TLBO algorithm. Detailed steps are introduced as follows:

Step1: Set parameters: the size of the population (N_p); set termination conditions, such as the maximum number of iteration steps G_{max}.

Step2: Initialize the class (population) and evaluate the individuals' knowledge level (fitness value).

Step3: Select the best individual as the teacher (X^T), and other individuals are called students (X^S). Calculate the mean of students, which is X^{mean}.

The formula for X^{mean} is as follows:

$$X^{mean} = \frac{\sum_i^{N_p} X^S}{N_p} \tag{A14}$$

Step 4: Teaching phase. Each student in the class is updated according to the difference between the teacher X^T and the mean of students X^{mean}:

$$X_i^{new} = X_i^{old} + r_i\left(X^T - T_F X^{mean}\right) \tag{A15}$$

$$\begin{cases} X_i^S = X_i^{new}, \; if \; f\left(X_i^{new}\right) \le f\left(X_i^{old}\right) \\ X_i^S = X_i^{old}, \; if \; f\left(X_i^{new}\right) > f\left(X_i^{old}\right) \end{cases} \tag{A16}$$

where r_i is a random factor, and T_F is the teaching factor. The calculation formula is as follows:

$$r_i = rand(1) \tag{A17}$$

$$T_F = round[1 + rand(0,1)\{2-1\}] \tag{A18}$$

Step 5: Learning phase. Randomly select two students X_i^S and X_j^S in the class and let them learn from each other. They can update themselves according to the following formula:

$$\begin{cases} X_i^{S,G+1} = X_i^{S,G} + r_i\left(X_i^{S,G} - X_j^{S,G}\right), \text{ if } f\left(X_i^{S,G}\right) < f\left(X_j^{S,G}\right) \\ X_i^{S,G+1} = X_i^{S,G} + r_i\left(X_j^{S,G} - X_i^{S,G}\right), \text{ if } f\left(X_i^{S,G}\right) \geq f\left(X_j^{S,G}\right) \end{cases} \tag{A19}$$

Step 6: Determine whether the convergence condition is satisfied. If it is satisfied, the optimization process ends; otherwise, return to Step 3, and continue the process.

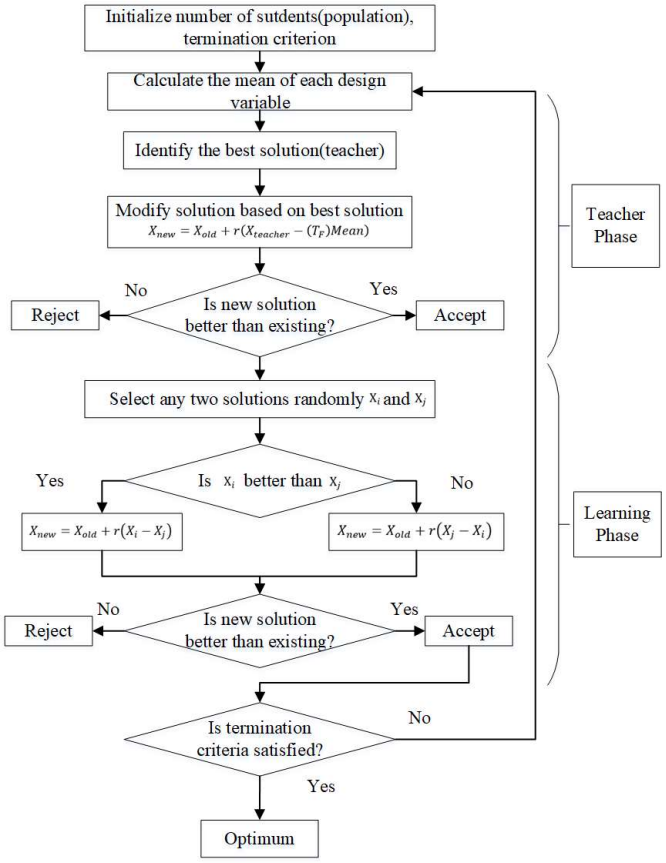

Figure A8. The framework of the TLBO algorithm.

Appendix C. The Introduction of the DO Framework and SBO Framework

DO and SBO frameworks are used to compare the optimization effects of the SAO framework. A DO framework directly invokes CFD simulation combined with algorithms to search for optimal aerodynamic shape parameters. The optimization process is shown in Figure A9. It has the advantage of being simple to implement. It is mostly used in gradient-based optimization algorithms, such as adjoint-based optimization. However, the heuristic algorithm is inefficiently optimized for this framework.

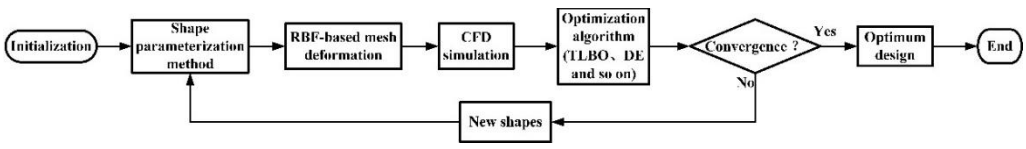

Figure A9. Direct optimization framework.

Since the direct optimization requires a large number of CFD simulations, which takes a lot of computing time, to improve computational efficiency, surrogate-based optimization

framework replaces many CFD simulations by building surrogate models. SBO frameworks are the most popular gradient-free methods. The main objective of SBO is to establish an approximate surrogate model equivalent to the expensive CFD in the design space by the design of experiments (DOE); then, a global optimization algorithm optimizes the approximate surrogate model for ASO. It looks for optimization directions through adaptive iteration until the surrogate model converges to a local or global optimal solution. However, this method is highly dependent on the accuracy of the surrogate model. Using different designs of experiments to select sample points will lead to different accuracies of the surrogate model, which will affect the optimization efficiency.

The SBO used in the paper is an adaptive SBO framework. This framework can build surrogate models with fewer initial sample data. The sample database of the initial surrogate model is obtained by CFD simulations of the initial wing shape. Then, the surrogate model is updated by the infilling strategy. As for the infilling strategy, it can combine the information in the sample database to predict the efficient position of the infilling point. We adopt the infilling strategy that the optimal design point is added to, to update the surrogate model. Latin hypercube sampling and uniform design methods are widely used in the infilling process. When the value difference between the newly added sample point and the optimal sample point is less than the set threshold, the optimization can be terminated. Figure A10 shows the SBO framework process.

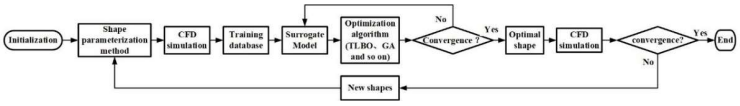

Figure A10. Surrogate-based optimization framework.

Appendix D. The Introduction of Kriging Model

The Kriging model is an interpolation model. For known sample datasets:

$$\boldsymbol{y}_S = \left[y\left(\boldsymbol{x}^{(1)}\right)\ y\left(\boldsymbol{x}^{(2)}\right)\cdots\ y\left(\boldsymbol{x}^{(n)}\right)\right]^T \tag{A20}$$

The Kriging model expresses its interpolation as:

$$\hat{y}(\boldsymbol{x}) = \sum_{i=1}^{n} \omega^{(i)} y^{(i)} \tag{A21}$$

To calculate the weight coefficient, the Kriging model regards the unknown function as a concrete realization of a Gaussian static random process, which is defined as:

$$Y(\boldsymbol{x}) = \beta_0 + Z(\boldsymbol{x}) \tag{A22}$$

where β_0 represents the mathematical expectation of $Y(\boldsymbol{x})$, $Z(\boldsymbol{x})$ is a static random process.

The Kriging model seeks the optimal weighting coefficient to minimize the mean square error:

$$MSE[\hat{y}(\boldsymbol{x})] = E\left[\left(\boldsymbol{\omega}^{\boldsymbol{T}}\boldsymbol{Y}_{\boldsymbol{S}} - Y(\boldsymbol{x})\right)^{2)}\right] \tag{A23}$$

At the same time, the interpolation condition should be met:

$$E\left[\sum_{i=1}^{n} \omega^{(i)} Y\left(\boldsymbol{x}^{(i)}\right)\right] = E[Y(\boldsymbol{x})] \tag{A24}$$

The Lagrange multiplier method is used to derive ω given by the following equations:

$$\begin{cases} \sum_{j=1}^{n} \omega^{(i)} R\left(\boldsymbol{x}^{(i)}, \boldsymbol{x}^{(j)}\right) + \frac{\mu}{2\sigma^2} = R\left(\boldsymbol{x}^{(i)}, \boldsymbol{x}\right) \\ \sum_{i=1}^{n} \omega^{(i)} = 1 \end{cases} \tag{A25}$$

It can be written in matrix form and solved to obtain:

$$\hat{y}(\boldsymbol{x}) = \beta_0 + \boldsymbol{r}^{\boldsymbol{T}}(x)\boldsymbol{R}^{-1}(y_S - \beta_0 \boldsymbol{F}) \tag{A26}$$

where

$$r = \begin{bmatrix} R\left(x^{(i)}, x\right) \\ \vdots \\ R\left(x^{(n)}, x\right) \end{bmatrix}$$

$$R = \begin{bmatrix} R\left(x^{(1)}, x^{(1)}\right) & \cdots & R\left(x^{(1)}, x^{(n)}\right) \\ \vdots & \ddots & \vdots \\ R\left(x^{(n)}, x(1)\right) & \cdots & R\left(x^{(n)}, x^{(n)}\right) \end{bmatrix}$$

$$F = [1\,1\,\cdots 1]^T$$

References

1. Chen, W.; Li, X.; Zhang, W. Shape optimization to suppress the lift oscillation of flow past a stationary circular cylinder. *Phys. Fluids* **2019**, *31*, 063604. [CrossRef]
2. Baker, A.J. On mathematics of physics of fluids maturation. *Phys. Fluids* **2021**, *33*, 081301. [CrossRef]
3. Kim, H.J.; Sasaki, D.; Obayashi, S.; Nakahashi, K. Aerodynamic optimization of supersonic transport wing using unstructured adjoint method. *AIAA J.* **2001**, *39*, 1011–1020. [CrossRef]
4. Wu, P.; Wang, P.; Gao, H. Dynamic mode decomposition analysis of the common research model with adjoint-based gradient optimization. *Phys. Fluids* **2021**, *33*, 035123. [CrossRef]
5. Srinath, D.N.; Mittal, S. An adjoint method for shape optimization in unsteady viscous flows. *J. Comput. Phys.* **2010**, *229*, 1994–2008. [CrossRef]
6. Papadimitriou, D.I.; Papadimitriou, C. Aerodynamic shape optimization for minimum robust drag and lift reliability constraint. *Aerosp. Sci. Technol.* **2016**, *55*, 24–33. [CrossRef]
7. Tang, Z.L.; Periaux, J. Uncertainty based robust optimization method for drag minimization problems in aerodynamics. *Comput. Methods Appl. Mech. Eng.* **2012**, *217*, 12–24. [CrossRef]
8. Nemec, M.; Aftosmis, M. Parallel Adjoint Framework for Aerodynamic Shape Optimization of Component-Based Geometry. In Proceedings of the 49th AIAA Aerospace Sciences Meeting including the New Horizons Forum and Aerospace Exposition, Orlando, FL, USA, 4–7 January 2011.
9. Zymaris, A.S.; Papadimitriou, D.I.; Giannakoglou, K.C.; Othmer, C. Adjoint wall functions: A new concept for use in aerodynamic shape optimization. *J. Comput. Phys.* **2010**, *229*, 5228–5245. [CrossRef]
10. Tang, X.; Luo, J.Q.; Liu, F. Aerodynamic shape optimization of a transonic fan by an adjoint-response surface method. *Aerosp. Sci. Technol.* **2017**, *68*, 26–36. [CrossRef]
11. Queipo, N.V.; Haftka, R.T.; Shyy, W.; Goel, T.; Vaidyanathan, R.; Tucker, P.K. Surrogate-based analysis and optimization. *Prog. Aerosp. Sci.* **2005**, *41*, 1–28. [CrossRef]
12. Vavalle, A.; Qin, N. Iterative response surface based optimization scheme for transonic airfoil design. *J. Aircraft.* **2007**, *44*, 365–376. [CrossRef]
13. Glaz, B.; Goel, T.; Liu, L.; Friedmann, P.P.; Haftka, R.T. Multiple-Surrogate Approach to Helicopter Rotor Blade Vibration Reduction. *AIAA J.* **2009**, *47*, 271–282. [CrossRef]
14. Chen, S.K.; Xiong, Y.; Chen, W. Multiresponse and Multistage Metamodeling Approach for Design Optimization. *AIAA J.* **2009**, *47*, 206–218. [CrossRef]
15. Mackman, T.J.; Allen, C.B.; Ghoreyshi, M.; Badcock, K.J. Comparison of Adaptive Sampling Methods for Generation of Surrogate Aerodynamic Models. *AIAA J.* **2013**, *51*, 797–808. [CrossRef]
16. Liu, J.; Song, W.P.; Han, Z.H.; Zhang, Y. Efficient aerodynamic shape optimization of transonic wings using a parallel infilling strategy and surrogate models. *Struct. Multidiscip. Optim.* **2017**, *55*, 925–943. [CrossRef]
17. Leifsson, L.; Koziel, S. Aerodynamic shape optimization by variable-fidelity computational fluid dynamics models: A review of recent progress. *J. Comput. Sci.-Neth.* **2015**, *10*, 45–54. [CrossRef]
18. Tesfahunegn, Y.A.; Koziel, S.; Leifsson, L.; Bekasiewicz, A. Surrogate-Based Airfoil Design with Space Mapping and Adjoint Sensitivity. In Proceedings of the 15th Annual International Conference on Computational Science (ICCS), Reykjavik University, Reykjavik, Iceland, 1–3 June 2015; pp. 795–804.
19. Giannakoglou, K.C.; Giotis, A.P.; Karakasis, M.K. Low-cost genetic optimization based on inexact pre-evaluations and the sensitivity analysis of design parameters. *Inverse Probl. Sci. Eng.* **2001**, *9*, 389–412. [CrossRef]

20. Karakasis, M.K.; Giotis, A.P.; Giannakoglou, K.C. Inexact information aided, low-cost, distributed genetic algorithms for aerodynamic shape optimization. *Int. J. Numer. Methods Fluids* **2003**, *43*, 1149–1166. [CrossRef]
21. Giannakoglou, K.C. Design of optimal aerodynamic shapes using stochastic optimization methods and computational intelligence. *Prog. Aerosp. Sci.* **2002**, *38*, 43–76. [CrossRef]
22. Praveen, C.; Duvigneau, R. Low cost PSO using metamodels and inexact pre-evaluation: Application to aerodynamic shape design. *Comput. Methods Appl. Mech. Eng.* **2009**, *198*, 1087–1096. [CrossRef]
23. Pehlivanoglu, Y.V.; Yagiz, B. Aerodynamic design prediction using surrogate-based modeling in genetic algorithm architecture. *Aerosp. Sci. Technol.* **2012**, *23*, 479–491. [CrossRef]
24. Liao, P.; Song, W.; Du, P.; Zhao, H. Multi-fidelity convolutional neural network surrogate model for aerodynamic optimization based on transfer learning. *Phys. Fluids* **2021**, *33*, 127121. [CrossRef]
25. Rao, R.V.; Savsani, V.J.; Vakharia, D.P. Teaching-Learning-Based Optimization: An optimization method for continuous non-linear large scale problems. *Inf. Sci.* **2012**, *183*, 1–15. [CrossRef]
26. Rao, R.V.; Kalyankar, V.D. Parameter optimization of modern machining processes using teaching-learning-based optimization algorithm. *Eng. Appl. Artif. Intell.* **2013**, *26*, 524–531. [CrossRef]
27. Cruz, N.C.; Redondo, J.L.; Alvarez, J.D.; Berenguel, M.; Ortigosa, P.M. A parallel Teaching-Learning-Based Optimization procedure for automatic heliostat aiming. *J. Supercomput.* **2017**, *73*, 591–606. [CrossRef]
28. Satapathy, S.C.; Naik, A. Modified Teaching-Learning-Based Optimization algorithm for global numerical optimization-A comparative study. *Swarm Evol. Comput.* **2014**, *16*, 28–37. [CrossRef]
29. Segura, C.; Coello, C.A.C.; Hernandez-Diaz, A.G. Improving the vector generation strategy of Differential Evolution for large-scale optimization. *Inf. Sci.* **2015**, *323*, 106–129. [CrossRef]
30. Qu, X.; Zhang, R.; Liu, B.; Li, H. An improved TLBO based memetic algorithm for aerodynamic shape optimization. *Eng. Appl. Artif. Intel.* **2017**, *57*, 1–15. [CrossRef]
31. Wu, X. Data-driven teaching–learning-based optimization (DTLBO) framework for expensive engineering problems. *Struct. Multidiscip. Optim.* **2021**, *64*, 2577–2591. [CrossRef]
32. Jameson, A. Optimum aerodynamic design using CFD and control theory CFD and control theory, AIAA Paper 95-1729. In Proceedings of the AIAA 12th Computational Fluid Dynamics Conference, San Diego, CA, USA, 19–22 June 1995.
33. Oyama, A.; Obayashi, S.; Nakahashi, K.; Hirose, N. Aerodynamic wing optimization via evolutionary algorithms based on structured coding. *Comput. Fluid Dyn. J.* **2000**, *8*, 570–577.
34. Wang, X.; Gao, Z. Genetic algorithm-based airfoil aerodynamic shape optimization design. *J. Aerodyn.* **2000**, *18*, 324–329. (In Chinese)
35. Epstein, B.; Peigin, S. Optimization of 3D wings based on Navier-Stokes solutions and genetic algorithms. *Int. J. Comput. Fluid Dyn.* **2006**, *20*, 75–92. [CrossRef]
36. Li, D.; Xia, L. Improved particle swarm optimization algorithm for pneumatic Application in design. *J. Aeronaut.* **2012**, *33*, 1809–1816. (In Chinese)
37. Rogalsky, T.; Derksen, R.W.; Kocabiyik, S. Differential evolution in aerodynamic optimization. In Proceedings of the 46th Annual Conference of Canadian Aeronautics and Space Institute, Montreal, QC, Canada, 3–5 May 1999; pp. 29–36.
38. Wang, X.; Damodaran, M. Aerodynamic Shape Optimization Using Computational Fluid Dynamics and Parallel Simulated Annealing Algorithms. *AIAA J.* **2001**, *39*, 1500–1508. [CrossRef]
39. Muyl, F.; Dumas, L.; Herbert, V. Hybrid method for aerodynamic shape optimization in the automotive industry. *Comput. Fluids* **2004**, *33*, 849–858. [CrossRef]
40. Kim, H.J.; Liou, M.S. Aerodynamic Optimization Using a Hybrid MOGA-Local Search Method. In Proceedings of the 54th Structural Dynamics, and Materials Conference, Boston, MA, USA, 8–11 April 2013.
41. Yiu, K.F.C.; Liu, Y.; Teo, K.L. A hybrid descent method for global optimization. *J. Glob. Optim.* **2004**, *28*, 229–238. [CrossRef]
42. Shahrokhi, A.; Jahangirian, A. Airfoil shape parameterization for optimum Navier–Stokes design with genetic algorithm. *Aerosp. Sci. Technol.* **2007**, *11*, 443–450. [CrossRef]
43. Kharal, A.; Saleem, A. Neural networks based airfoil generation for a given using Bezier–PARSEC parameterization. *Aerosp. Sci. Technol.* **2012**, *23*, 330–344. [CrossRef]
44. Ebrahimi, M.; Jahangirian, A. Aerodynamic Optimization of Airfoils Using Adaptive Parameterization and Genetic Algorithm. *J. Optim. Theory. Appl.* **2013**, *162*, 257–271. [CrossRef]
45. Kulfan, B.; Bussoletti, J. "Fundamental" Parameteric Geometry Representations for Aircraft Component Shapes. In Proceedings of the 11th AIAA/ISSMO Multidisciplinary Analysis and Optimization Conference, Portsmouth, VA, USA, 6–8 September 2006.
46. Lassila, T.; Rozza, G. Parametric free-form shape design with PDE models and reduced basis method. *Comput. Methods Appl. Mech. Eng.* **2010**, *199*, 1583–1592. [CrossRef]
47. Gagnon, H.; Zingg, D.W. Two-Level Free-Form and Axial Deformation for Exploratory Aerodynamic Shape Optimization. *AIAA J.* **2015**, *53*, 2015–2026. [CrossRef]
48. Wu, X.J.; Zhang, W.W.; Peng, X.H.; Wang, Z.Y. Benchmark aerodynamic shape optimization with the POD-based CST airfoil parametric method. *Aerosp. Sci. Technol.* **2019**, *84*, 632–640. [CrossRef]
49. Jakobsson, S.; Amoignon, O. Mesh deformation using radial basis functions for gradient-based aerodynamic shape optimization. *Comput. Fluids* **2007**, *36*, 1119–1136. [CrossRef]

50. Poirier, V.; Nadarajah, S. Efficient Reduced-Radial Basis Function-Based Mesh Deformation Within an Adjoint-Based Aerodynamic Optimization Framework. *J. Aircraft.* **2016**, *53*, 1905–1921. [CrossRef]
51. Wu, X.J.; Zhang, W.W.; Song, S.F. Robust aerodynamic shape design based on an adaptive stochastic optimization framework. *Struct. Multidiscip. Optim.* **2018**, *57*, 639–651. [CrossRef]
52. Zhang, W.W.; Li, X.T.; Ye, Z.Y.; Jiang, Y.W. Mechanism of frequency lock-in in vortex-induced vibrations at low Reynolds numbers. *J. Fluid Mech.* **2015**, *783*, 72–102. [CrossRef]
53. Zhang, W.W.; Gao, C.Q.; Liu, Y.L.; Ye, Z.Y.; Jiang, Y.W. The interaction between flutter and buffet in transonic flow. *Nonlinear Dyn.* **2015**, *82*, 1851–1865. [CrossRef]
54. Wang, H.T.; Zhu, X.C.; Du, Z.H. Aerodynamic optimization for low pressure turbine exhaust hood using Kriging surrogate model. *Int. Commun. Heat Mass.* **2010**, *37*, 998–1003. [CrossRef]
55. Han, Z.H.; Zimmermann, R.; Gortz, S. Alternative Cokriging Model for Variable-Fidelity Surrogate Modeling. *AIAA J.* **2012**, *50*, 1205–1210. [CrossRef]
56. Tesfahunegn, Y.A.; Koziel, S.; Gramanzini, J.-R.; Hosder, S.; Han, Z.-H.; Leifsson, L. Application of Direct and Surrogate-Based Optimization to Two-Dimensional Benchmark Aerodynamic Problems: A Comparative Study. In Proceedings of the 53rd AIAA Aerospace Science Meeting, Kissimmee, FL, USA, 5–9 January 2015.
57. Lee, C.; Koo, D.; Telidetzki, K.; Buckley, H.; Gagnon, H.; Zingg, D.W. Aerodynamic Shape Optimization of Benchmark Problems Using Jetstream. In Proceedings of the 53rd AIAA Aerospace Science Meeting, Kissimmee, FL, USA, 5–9 January 2015.
58. Ren, J.; Thelen, A.S.; Amrit, A.; Du, X.; Leifsson, L.T.; Tesfahunegn, Y.; Koziel, S. Application of Multifidelity Optimization Techniques to Benchmark Aerodynamic Design Problems. In Proceedings of the 54th AIAA Aerospace Sciences Meeting, San Diego, CA, USA, 4–8 January 2016.
59. Leifsson, L.T.; Koziel, S.; Hosder, S. Aerodynamic Design Optimization: Physics-based Surrogate Approaches for Airfoil and Wing Design. In Proceedings of the 52nd Aerospace Sciences Meeting, National Harbor, MD, USA, 13–17 January 2014.
60. Zhang, Y.; Han, Z.-H.; Shi, L.; Song, W.-P. Multi-round Surrogate-based Optimization for Benchmark Aerodynamic Design Problems. In Proceedings of the 54th AIAA Aerospace Sciences Meeting, San Diego, CA, USA, 4–8 January 2016.
61. Iuliano, E. Global optimization of benchmark aerodynamic cases using physics-based surrogate models. *Aerosp. Sci. Technol.* **2017**, *67*, 273–286. [CrossRef]
62. He, X.L.; Li, J.C.; Mader, C.A.; Yildirim, A.; Martins, J.R. A Martins. Robust aerodynamic shape optimization-From a circle to an airfoil. *Aerosp. Sci. Technol.* **2019**, *87*, 48–61. [CrossRef]